JACS
JOURNAL OF THE AMERICAN CHEMICAL SOCIETY

ARTICLE

pubs.acs.org/JACS

Modulation of the Photocycle of a LOV Domain Photoreceptor by the Hydrogen-Bonding Network

Sarah Raffelberg,[†] Madina Mansurova,[†] Wolfgang Gärtner,[†] and Aba Losi[*,†,§]

[†]Max-Planck-Institute for Bioinorganic Chemistry, Stiftstrasse 34-36, 45470 Mülheim, Germany
[§]Department of Physics, University of Parma, viale G.P. Usberti 7/A, 43100 Parma, Italy

Supporting Information

ABSTRACT: An extended hydrogen-bonding (HB) network stabilizes the isoalloxazine ring of the flavin mononucleotide (FMN) chromophore within the photosensing LOV domain of blue-light protein receptors, via interactions between the C(2)=O, N(3)H, C(4)=O, and N(5) groups and conserved glutamine and asparagine residues. In this work we studied the influence of the HB network on the efficiency, kinetics, and energetics of a LOV protein photocycle, involving the reversible formation of a FMN−cysteine covalent adduct. The following results were found for mutations of the conserved amino acids N94, N104, and Q123 in the *Bacillus subtilis* LOV protein YtvA: (i) Increased (N104D, N94D) or strongly reduced (N94A) rate of adduct formation; this latter mutation extends the lifetime of the flavin triplet state, i.e., adduct formation, more than 60-fold, from 2 μs for the wild-type (WT) protein to 129 μs. (ii) Acceleration of the overall photocycle for N94S, N94A, and Q123N, with recovery lifetimes 20, 45, and 85 times faster than for YtvA-WT, respectively. (iii) Slight modifications of FMN spectral features, correlated with the polarization of low-energy transitions. (iv) Strongly reduced (N94S) or suppressed (Q123N) structural volume changes accompanying adduct formation, as determined by optoacoustic spectroscopy. (v) Minor effects on the quantum yield, with the exception of a considerable reduction for Q123N, i.e., 0.22 vs 0.49 for YtvA-WT. The data stress the importance of the HB network in modulating the photocycle of LOV domains, while at the same time establishing a link with functional responses.

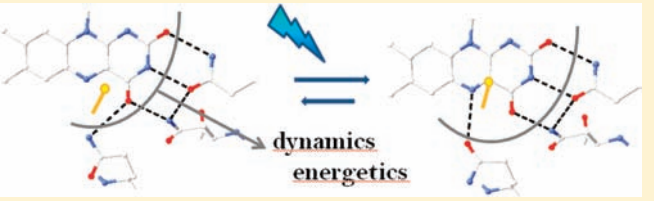

INTRODUCTION

The photocycle of LOV (light, oxygen, voltage) protein domains is chiefly dictated by the photophysical and photochemical properties of the bound flavin mononucleotide (FMN) chromophore[1] but also influenced by the surrounding microenvironment.[2,3] Weak interactions, such as hydrogen-bonding (HB), and spatial constraints imposed by the side chains of amino acids forming the FMN binding cavity are expected to affect the kinetics, the energetics, and the efficiency of the different steps of the photocycle. In this respect the hydrogen bonds formed around the polar groups of the FMN isoalloxazine could be of primary importance, besides being a major determinant in chromophore stabilization and the first protein−chromophore interface undergoing conformational changes upon light activation.[4−8]

LOV domains are small photosensing protein modules of ca. 100 amino acids forming a quite compact and structurally conserved α/β core flanked by variable N- and C-terminal helical regions.[9−11] They host FMN as a non-covalently bound chromophore and absorb maximally around 450 nm (resting or dark-adapted state, referred to as LOV_{447}), and they constitute a subclass of the PAS (PerArntSim) superfamily.[12] According to a recently proposed nomenclature,[13] we assign the following secondary structure elements to the LOV core (from the N-terminal part): AβBβCαDαEαFαGβHβI. LOV domains are the photochemically active moiety of LOV proteins, a class of blue-light (BL) photoreceptors comprising, among others, plant phototropins (phot),[9] the fungal protein VIVID,[14] and a growing number of prokaryotic photoresponsive proteins.[11,15−21] The photochemistry of LOV domains, first elucidated for phot and afterward for a variety of bacterial and fungal proteins, involves the formation of a FMN−cysteine C(4a)−thiol adduct, significantly blue-shifted with respect to the dark state and non-fluorescent (referred to as LOV_{390}), generated via the short microsecond decay of the FMN triplet state.[1,22,23] In LOV_{390}, a covalent bond is formed between the carbon atom at position 4a and the thiol group of a conserved cysteine localized in the Dα−Eα loop (Figure 1 provides structural views of the chromophore and its protein surroundings for both the parent state and the photoadduct; amino acid numbering herein refers to YtvA from *Bacillus subtilis*). LOV_{390} reverts in the dark to the unphotolyzed state (LOV_{447}) on a time scale ranging from a few seconds to many hours at room temperature.[1,24−27] Importantly, the recovery is accelerated by imidazole, suggesting a base-catalyzed reaction.[28,29] Furthermore, pH,[23,29] deuterium effects,[22,30] and structural studies indicate that a proton-transfer reaction from N(5) is the rate-limiting step for the dark recovery reaction.

Received: November 12, 2010
Published: March 16, 2011

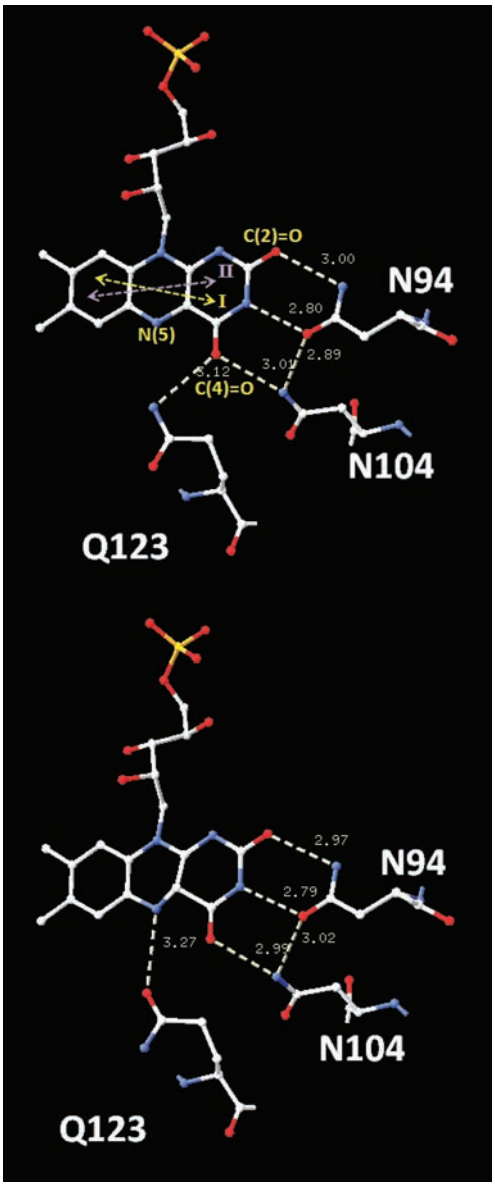

Figure 1. Hydrogen-bonding network of YtvA-LOV investigated in this work, in the (top) dark-adapted and (bottom) light-activated (photoadduct) states (PDB coordinates from 2pr5 and 2pr6). For the dark state we show the calculated polarization directions of the low-energy electronic transitions: I, blue-light range, λ_{max} ~450 nm; II, UVA range, λ_{max} ~350 nm (modified from ref 41, but see also ref 42 for an experimental determination). The atoms of FMN involved in the HB network studied here are shown in yellow.

Nevertheless, despite this well-established photocycle, the details for both LOV_{390} formation from the triplet state and its reversion are still a matter of debate,[31−33] as is the molecular basis of the dramatically different photocycle kinetics in different proteins. In this respect, understanding how the microenvironment surrounding the chromophore influences the photocycle, i.e., the effects of protein−chromophore interactions, is of crucial importance. Furthermore, modulation of the photocycle might turn out to be a very important aspect for BL photoreceptor-based optogenetic applications, by tuning the kinetics and yielding the requirements of the particular cell system and/or metabolic process of interest.[34−37]

Recently, a series of mutations have been designed to alter steric restrictions in the vicinity of the 8α-methyl group at the xylene side of FMN in *Avena sativa* phot1-LOV2 domain of phototropin 1 (*As*phot1-LOV2) and studied by means of proton ENDOR and optical spectroscopy.[3] Asn 425, localized within the Aβ−Bβ loop, appears to have a significant influence on the recovery lifetime of the adduct, which decreased from 48 s in the wild-type (WT) protein to 7.5 s in *As*phot1-LOV2-N425C. Interaction between Asn425 and the 8α-methyl group appears to force the isoalloxazine ring into a precise conformation, thus stabilizing the cysteinyl−C(4a) adduct. Another important residue influencing the kinetics of the photocycle that stabilize the photoadduct through steric effects is Ile427 (I39 in YtvA) on strand Bβ of *As*phot1-LOV2.[2] Nevertheless, in that case the 2-fold slower formation and 10-fold faster decay of the photoadduct by removing the δ-carbon of the isoleucine chain (I427V mutation) are not due to direct interaction of Ile427 with FMN but rely on van der Waals contact between a CH_2 group and the nearby sulfur of the reactive cysteine. The corresponding substitution I403V has been recently used to achieve a very fast photocycle in *Arabidopsis thaliana* (*At*) phot1-LOV2, in order to productively allow Fourier transform infrared (FTIR) step-scan measurements of chromophore and protein dynamics during formation of the photoadduct.[32] Further, mutations of residues interacting with the ribityl chain of FMN have been shown to affect the recovery reaction[38,39] by as much as 2 orders of magnitude.[27] Recently, a double mutation of YtvA, I39V/F46H, was demonstrated to accelerate 75-fold the recovery reaction, although the two residues are not directly interacting with the chromophore.[34] In particular, F46 undergoes a light-induced flipping, suggesting that this region of the protein is particularly flexible.[7,34]

An alternative approach has been recently reported by Mansurova et al., who exchanged the native chromophore with sterically modified flavins as chromophores via a chromophore exchange protocol.[40] Also in those experiments, the tight interactions between the chromophore and the protein were documented as a change of this interplay that significantly alters the thermal recovery kinetics.[40]

Here we focus instead on the HB network between the N(5), C(4)═O, N(3)H, and C(2)═O positions of the isoalloxazine moiety of FMN and an ensemble of conserved polar, uncharged amino acids (Figure 1). The hydrogen bonds at these positions of the chromophore undergo changes after blue-light absorption, as was recently documented in detail by means of advanced infrared spectroscopy techniques.[8,31,32,43] In particular, hydrogen bonds at C(2)═O and C(4)═O are weakened upon formation of the adduct, to somewhat different extents in different LOV systems.[8,44−46] In YtvA, the *B. subtilis* LOV protein investigated here, the three involved amino acids are Asn94, Asn104, and Gln123 (Figure 1; in the following we will refer to the amino acid coding of YtvA from *B. subtilis*).

Our study was prompted by formerly reported observations that hydrogen bonds affect not only the UV−vis absorption spectrum of riboflavin but also its photoreactivity.[47,48] In particular, H-bonding at N(1), C(2)═O, N(3)H, and C(4)═O was shown to increase the rate of hydrogen abstraction from a donor substrate, thus facilitating flavin reduction, when the riboflavin derivative was converted to its triplet state.[48] A theoretical investigation, based on quantum mechanics/molecular mechanics (QM/MM) methods applied to lumiflavin, has contributed to our knowledge of the influence that the HB network

exerts on the low-lying excited state of the flavin cofactor, indicating that the protein microenvironment enables participation of the ($n\pi^*$) states in the decay processes of the lowest ($\pi\pi^*$) excited singlet state (transition I in Figure 1), i.e., by enhancing singlet−triplet spin−orbit coupling.[49] Mutations of the three conserved polar residues that chiefly contribute to the HB network within the FMN binding pocket are thus expected to affect the photocycle kinetics, efficiency, and/or energetics. Indeed, it was shown recently that mutation of Q513 in *As*phot1-LOV2 (Q123 in YtvA) can strongly affect the recovery reaction kinetics.[50] Furthermore, N94, N104, and Q123 belong to the β-scaffold of the LOV core (strands Gβ, Hβ, and Iβ, respectively), participating in light-to-signal transmission, probably with the intervention of helical regions flanking the LOV core.[7,10,32,39,51,52] In particular, the conserved glutamine on strand Iβ (here Q123) was recently identified as a potential switch to convey light-triggered conformational changes from the chromophore cavity to the LOV domain surface, e.g., Q575 in *At*phot1-LOV2,[53] Q513 in *As*phot1-LOV2,[50] Q182 in the fungal protein VIVID,[51] and Q1029 in *Adiantum capillus veneris Ac*phy3-LOV2.[43] The mechanism underlying the conformational change effects resides in the fact that formation of the thioether bond in the adduct reduces the flavin ring and protonates N(5).[31] In order to maintain HB with N(5)H, this requires that the lateral chain of Q123 must flip in the lit state, as suggested by the structural data of several LOV domains.[4,5,7,10,51] Time-resolved FTIR spectroscopy has demonstrated that the Gln flipping, with loss of HB, is completed within a few microseconds, concomitant with formation of the adduct.[32] This flipping is then reversed, with recovery of the dark state and breakage of the covalent FMN−Cys bond. A link between this glutamine-based conformational switch and *in vivo* effects is indicated by the lack of light activation of the stress factor σ^B with the mutated YtvA-Q123N in *B. subtilis*.[54] Furthermore, it has been reported that the mutation Q575L (on LOV2) attenuates light-induced self-phosphorylation in *At*phot1.[55] However, similar functional investigations have not been carried out for the positions (in YtvA) Asn94 and Asn104.

In this work we have investigated a series of mutations at Q123, N94, and N104 with the aim of characterizing the kinetics, efficiency, and energetics of the photocycle of YtvA proteins with an altered HB network around FMN, by means of steady-state spectroscopy, nanosecond flash photolysis, and time-resolved calorimetry. The aim of our investigation was twofold: first to assess the direct influence of the H-bonding situation of the chromophore on the photochemical and thermally driven steps, and second to understand the link between chromophore−protein interactions and signal propagations from the LOV core to domain/protein partners in the signal transduction chain. The outcome of our investigation will also be discussed in the frame of recently published experimental data on the mechanism of adduct formation and decay, and of possible extensions of the designed mutations for biotechnology applications.

MATERIALS AND METHODS

Mutagenesis, Protein Expression, and Purification. A total of seven new mutations were generated: Q123N, N94S, N94D, N94A, N104S, N104D, and N104A. Mutagenesis was performed by the QuikChange method (QuikChange II XL, Stratagene). The primer design was performed with PrimerX[56] using the option "DNA-based". The primer sequences suggested by this program were again inspected individually, before primers were ordered for mutagenesis (see Supporting Information for the primer sequencees). For all mutagenesis experiments, the obtained PCR products were treated with the restriction enzyme *Dpn*I (New England BioLabs). *Dpn*I is specific for methylated and hemimethylated DNA (targeting sequence: 5′-Gm^{6}ATC-3′) and is used to digest the parental DNA template in the PCR products. A 0.5 μL portion of *Dpn*I (20 000 U/mL) was added to each PCR product, and the digestion reaction was carried out at 37 °C for 30 min. In all cases, mutations were confirmed by sequencing.

Expression in *E. coli* (BL21) (Stratagene, Amsterdam, The Netherlands) yielded His-tagged, mutated proteins, using IPTG (BioMol, Hamburg, Germany) induction and employing the pET28a plasmid (Novagen-Merck, Darmstadt, Germany), as described.[57] The proteins were purified by affinity chromatography on a Talon resin (Qiagen, Hilden, Germany) and finally concentrated in sodium phosphate buffer 10 mM, NaCl 10 mM, pH = 8.

Steady-State and Transient Optical Spectroscopy. Absorbance spectra were recorded with a Jasco 7850 UV/vis spectrophotometer. Steady-state fluorescence measurements were carried out with a Perkin-Elmer LS50 luminescence spectrometer. The output signal was divided by the fraction of absorbed energy ($1-10^{-A}$, where A is the absorbance at the excitation wavelength) in order to obtain a signal that is proportional to the quantum yield.

Transient absorbance changes after nanosecond laser flash excitation were recorded using an LFP111 detection system (Luzchem, Ontario, Canada). For excitation, a Nd:YAG-driven tunable OPO laser was used (Nd:YAG, Innolas, Garching, Germany; OPO, GWU Lasertechnik, Erftstadt, Germany). The single-shot experiments were performed in the linear laser-energy dependence region of the transient absorbance changes with λ_{exc} = 450 nm. All measurements were done at 20 °C using 1 cm light-path quartz cuvettes. The data were handled and analyzed using Origin Professional version 5.0 (Microcal Software, Inc., Northampton, MA).

Arrhenius and Eyring plots for the dark recovery reaction of the photoadduct were built by recording the recovery of FMN fluorescence (λ_{ex} = 303 nm, λ_{em} = 500 nm). The kinetics traces were fitted with a mono- or bi-exponential function, furnishing the recovery lifetime (τ_{rec}) as a function of temperature, in the range of the protein stability (11−25 °C). Excitation was at 303 nm, in order to minimize secondary photochemistry leading to the formation of the photoproduct during recording of the traces.[39]

Laser-Induced Optoacoustic Spectroscopy (LIOAS). For the LIOAS experiments, excitation at 450 nm was achieved by pumping the frequency-tripled pulse of a Nd:YAG laser (SL 456G, 6-ns pulse duration, 355 nm, Spectron Laser System, Rugby, Great Britain) into a β-barium borate optical parametric oscillator (OPO-C-355, bandwidth 420−515 nm, GWU Lasertechnik, Erftstadt, Germany) as previously described.[58,59] The FLASH 100 cuvette holder (Quantum Northwest Inc., Spokane, WA) was temperature-controlled to ±0.02 °C. The signal was detected by a V103-RM ultrasonic transducer and fed into a 5662 preamplifier (Panametrics Inc., Waltham, MA). The pulse fluence was varied with a neutral density filter and measured with a pyroelectric energy meter (RJP735 head connected to an RJ7620 meter from Laser Precision Corp.). The beam was shaped by a 1 × 12 mm slit, allowing a time resolution of ~60 ns by using deconvolution techniques.[60] The experiments were performed in the linear regime of amplitude versus laser fluence, and the total incident energy normally used was ~40 μJ/pulse (corresponding to 15×10^{-11} einstein for 450 nm excitation, photon energy 265.8 kJ/mol). The sample concentration was about 15 μM, giving 1.8×10^{-9} mol in the excitation volume V_0 = 0.12 mL. These conditions correspond to a ratio of 0.08 photon per protein molecule. New coccine (Fluka, Neu-Ulm, Germany) was used as calorimetric

reference.[61] The time evolution of the pressure wave was assumed to be a sum of monoexponential functions. The deconvolution analysis yielded the fractional amplitudes (φ_i) and the lifetimes (τ_i) of the transients (Sound Analysis 3000, Quantum Northwest Inc.). The time window was between 20 ns and 5 μs. At a given temperature and for each resolved ith step, the fractional amplitude φ_i is the sum of the fraction of absorbed energy released as heat (α_i) and the structural volume change per absorbed einstein (ΔV_i), according to eq 1:[62,63]

$$\varphi_i = \alpha_i + \frac{\Delta V_i}{E_\lambda}\frac{c_p\rho}{\beta} \quad (1)$$

where E_λ is the molar excitation energy, $\beta = (\partial V/\partial T)_p\Delta V$ is the volume expansion coefficient, c_p is the heat capacity at constant pressure, and ρ is the mass density of the solvent. In this work we used the so-called "two temperature" method in order to separate α_i from ΔV_i.[64] The sample waveform was acquired at a temperature for which heat transport is zero, $T_{\beta=0}$ = 3.2 °C, and at a slightly higher temperature, $T_{\beta>0}$ = 10 °C. At $T_{\beta=0}$, the LIOAS signal is only due to ΔV_i. The reference for deconvolution was recorded at $T_{\beta>0}$, and eqs 2a and 2b were then used to derive α_i and ΔV_i:

$$\Phi_i\Delta V_i = \varphi_i|_{T_{\beta=0}} \times E_\lambda\frac{\beta}{c_p\rho}\bigg|_{T_{\beta>0}} \quad (2a)$$

$$\alpha_i = \varphi_i|_{T_{\beta>0}} - \varphi_i|_{T_{\beta=0}} \quad (2b)$$

Photophysical Parameters and LIOAS Data Handling. The LIOAS signals for YtvA-WT and the mutated proteins were best fitted (with some exceptions, *vide infra*) by a two-exponential decay function as previously described.[57,59] The unresolved step (τ_1 < 20 ns) is assigned to the fast reactions resulting in the formation of the flavin triplet state (subscript T; this step is not time-resolved by LIOAS). The microsecond process (τ_2 = 2 μs for YtvA-WT) corresponds to the triplet decay with formation of the photoadduct (subscript 390, according to the approximate absorption maximum). Energy balance considerations and the results of deconvolution directly provide the products $\Phi_T E_T$ and $\Phi_{390}E_{390}$ (eqs 3a and 3b), referring to the quantum yield of formation for the triplet state and adduct, respectively, multiplied by the energy level of the two transient species:[65]

$$\Phi_T\frac{E_T}{E_\lambda} = 1 - \alpha_1 - \Phi_F\frac{E_F}{E_\lambda} \quad (3a)$$

$$\alpha_2 = \Phi_T\frac{E_T}{E_\lambda} - \Phi_{390}\frac{E_{390}}{E_\lambda} \quad (3b)$$

where E_F is the average energy for the fluorescence emission (232 kJ/mol), and E_λ (265.8 kJ/mol) is the photonic energy corresponding to λ_{ex} = 450 nm excitation wavelength. In this work we used $E_T \approx 200$ kJ/mol, as previously measured[38,57,66] to obtain Φ_T, and we estimated the energy content of the adduct after the independent determination of Φ_{390} (*vide infra*).[65]

The molecular volume changes that the system suffers upon formation of the flavin triplet state and of the photoadduct (with respect to the unphotolyzed state) are calculated with eqs 4a and 4b:

$$\Delta V_T = \frac{\Delta V_1}{\Phi_T} \quad (4a)$$

$$\Delta V_{390} = \Delta V_T + \frac{\Delta V_2}{\Phi_{390}} \quad (4b)$$

The fluorescence quantum yield, Φ_F of the bound flavin for the mutated proteins was measured at 20 °C, by comparison with YtvA-WT (Φ_F = 0.22) and FMN (Φ_F = 0.26), employing steady-state spectroscopy.[57,59,67] The value of Φ_{390} was estimated by recording the bleaching of the unphotolyzed state on the microsecond time scale, at 450 and 475 nm, after laser excitation at 450 nm, employing the laser flash photolysis instrumentation, and by comparison with YtvA-WT (Φ_{390} = 0.49),[57] assuming that the absorption coefficient of the mutated proteins remains unaltered.

RESULTS

Spectral Features and Light−Dark Difference Spectra. All the mutated proteins exhibit absorption spectra similar to that of YtvA-WT. The three major bands (blue, UVA, and UVB regions, transitions I, II, and III, respectively) undergo large light-induced changes upon formation of the photoadduct, well described by the light−dark (L-D) difference spectra, with a defined pattern of maxima and minima (Figure 2, Table 1).

The largest effects on the absorption spectra are produced by the Asn/Asp exchange at positions 94 and 104, and by the Q123N mutation (Figure 2 and Table 1). Replacing asparagine 104 with aspartate has an effect only on transition I (Figure 2a), inducing a blue-shift. In contrast, in YtvA-N94D a small blue-shift of transition I is accompanied by a larger red-shift of the UVA transition II (Figure 2b), accordingly polarized in the direction of C(2)=O and N(3)H. This UVA transition is in fact the most sensitive to the polarity and HB ability of the solvent[47,48,68] and shows the greatest variation among various LOV domains.[46,69] Interestingly, YtvA-Q123N shows a 3 nm blue-shift of the lowest energy transition with respect to YtvA-WT, whereas its fluorescence spectrum is virtually unaffected (Figure 3). A similar feature was recently described for mutations of glutamate 46 in the photoactive yellow protein and was predicted to arise from a broadening of the excited-state energy surface, although in our case the effects are very small.[70]

Photochemical Events: Triplet Decay and Formation of the Photoadduct. The most notable features of the micro-second time-resolved transient absorbance measurements (flash photolysis) are summarized in Table 2: (i) the faster formation of the adduct/decay of triplet state observed for YtvA-N94D, YtvA-N104D, and, to a lesser extent, also for YtvA-Q123N; (ii) the remarkable slowing down of the triplet decay/photoproduct formation in YtvA-N94A (Figure 4); and (iii) the smaller Φ_{390} for YtvA-Q123N (about half that for YtvA-WT).

The data curves could be readily interpolated by means of a mono-exponential decay (Table 2), with the exception of YtvA-N104A, for which the curve was better described by a bi-exponential decay (i.e., the χ^2 improved more than 10% with respect to a mono-exponential fitting).

Photocalorimetric (LIOAS) Experiments: Triplet Formation and Decay, Energetics, and Structural Changes. LIOAS experiments have been previously performed with YtvA-WT[57,59] and other LOV proteins.[38] Given the time scale and time resolution of LIOAS, the production of FMN triplet state and its decay into the adduct are readily recorded, but the former process cannot be time-resolved (τ_1 < 20 ns), and we see only the result of the sub-nanosecond reactions leading to triplet formation. The formation of the adduct can instead be followed in real time, provided that it occurs with a lifetime $\tau_2 \leq 5$ μs (Table 3).

The majority of the mutated proteins behave similarly to YtvA-WT, with some notable exceptions: (i) YtvA-Q123N does not show any structural volume change upon formation of the adduct, i.e., ΔV_2 = 0, although the heat released in this step is

dx.doi.org/10.1021/ja1097379 |J. Am. Chem. Soc. 2011, 133, 5346–5356

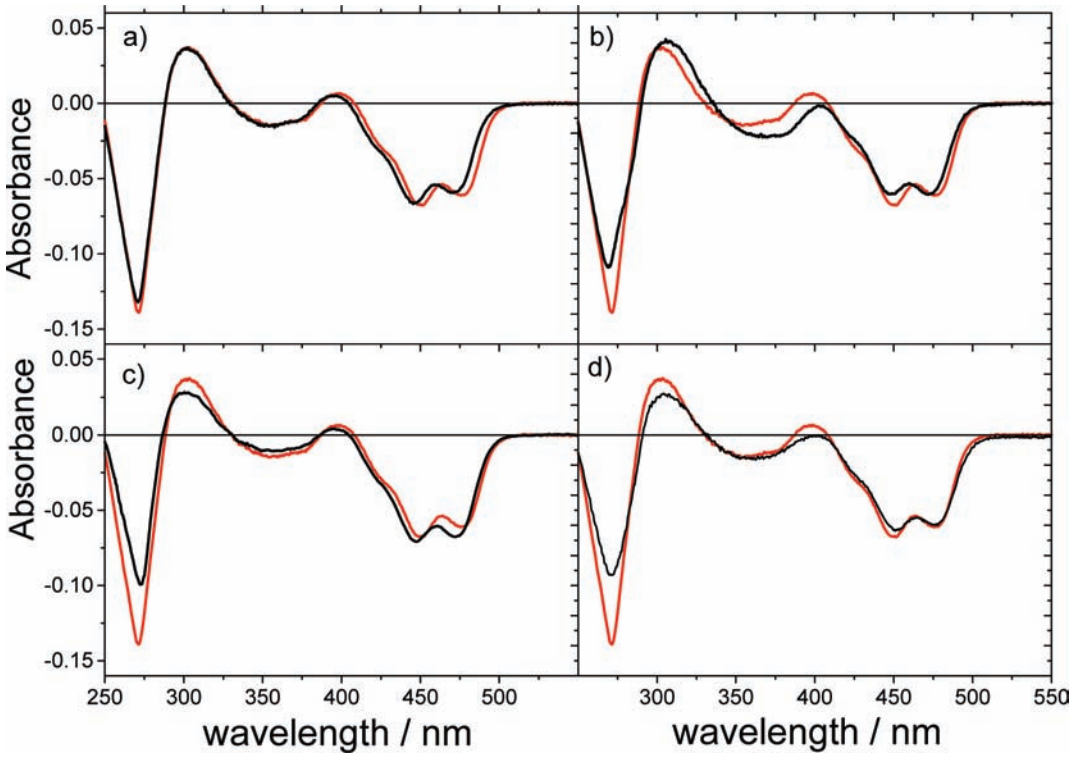

Figure 2. Light−dark difference absorption spectra for selected mutated YtvA proteins (black lines), compared to YtvA-WT (red line): (a) YtvA-N104D, (b) YtvA-N94D, (c) YtvA-Q123N, and (d) YtvA-N104S. See Table 1 for the maxima−minima patterns of all studied proteins.

Table 1. Absorption Light−Dark (L-D) Maxima and Minima and Fluorescence Parameters of YtvA Proteins

	L-D min/nm (parent state bleaching)[a]	L-D max/nm (photoadduct)[a]	fluorescence max/nm	Φ_F
YtvA-WT	272/354;374/450;477	398;302	497	0.22
YtvA-N94D	269/364;380/448;473	404;306	497	0.15
YtvA-N94A	271/355/449;477	386;306	501	0.25
YtvA-N94S	271/354;370/452;477	402;303	501	0.14
YtvA-N104D	272/335;361/446;472	396;302	494	0.22
YtvA-N104A	272/348/449;475	396;304	497	0.20
YtvA-N104S	271/354;374/451;477	398;302	501	0.20
YtvA-Q123N	273/350;373/447;473	396;300	496	0.27

[a] Transitions in the UVB, UVA, and blue light spectral regions are separated by "/"; shoulders and vibrational bands in the same spectral region are separated by ";".

well detectable with the correct time constant (Table 3 and Figure 5); (ii) ΔV_2 is strongly reduced in YtvA-N94S; and (iii) the formation of the adduct cannot be detected for YtvA-N94A, in agreement with the long lifetime of the triplet state (see Table 2).

The deconvolution of LIOAS waveforms thus provides the fraction of heat released (α_i) in each step and the lifetime of the triplet states; i.e., τ_2 in Table 3 should be the same as τ_T as recorded from transient absorption experiments (Table 2), provided that spectrally silent transitions do not occur on the same time scale. By performing temperature-dependent experiments, it is also possible to obtain the structural volume changes (ΔV_i, per mole of absorbed photons) that accompany each step (Table 3; eqs 2a, 2b, 3a, and 3b).

Equation 3a allows us to determine the triplet formation quantum yield, Φ_T, which is very similar among all the proteins investigated (Table 4), with the exception of YtvA-N104S, which has a higher value, $\Phi_T = 0.79$, underscored by the small fraction of released heat in the short nanosecond step (α_1 in Table 3).

The evaluation of E_{390} as the energy content of the photoadduct is negatively affected by the large errors associated in some cases with both Φ_{390} as determined by flash photolysis (Table 2) and the quantity $E_{390}\Phi_{390}$, independently determined by LIOAS. In at least two cases, YtvA-N104S and YtvA-Q123N, the energy stored in the signaling state appears larger with respect to YtvA-WT, i.e., close to the triplet energy level, $E_T \approx$ ca. 200 kJ/mol.[38,57,66]

The total contraction, ΔV_{390}, that the system suffers upon light activation (Table 4) is strongly reduced in YtvA-Q123N and YtvA-N94S. This is due to the fact that the volume change associated with the formation of the photoadduct is zero or close to zero, respectively, whereas the structural changes associated

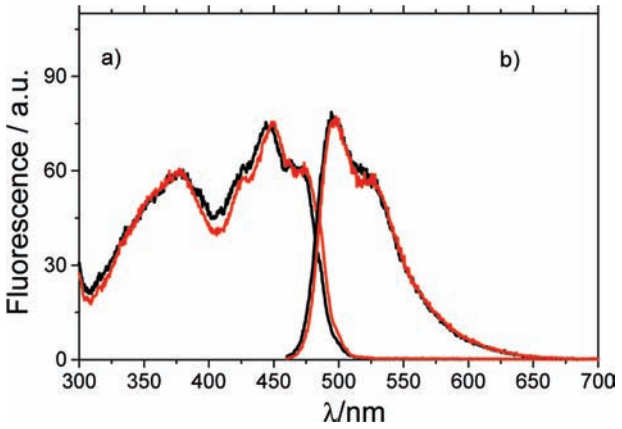

Figure 3. (a) Excitation (λ_{em} = 500 nm) and (b) emission (λ_{ex} = 450 nm) fluorescence spectra for YtvA-Q123N (black) and YtvA-WT (red). Note that the 3 nm blue-shift in the excitation spectrum (identical to that observed in absorbance) is not accompanied by a concomitant shift in the emission profile.

Table 2. Triplet Lifetimes and Photocycle Quantum Yields

	τ_T	Φ_{390}[a]
YtvA-WT	2.00 ± 0.20	0.49 ± 0.04
YtvA-N94D	1.34 ± 0.14	0.22 ± 0.09[b]
YtvA-N94A	129 ± 10	0.46 ± 0.05
YtvA-N94S	2.05 ± 0.14	0.51 ± 0.16
YtvA-N104D	1.27 ± 0.12	0.47 ± 0.30
YtvA-N104A	2.50 ± 0.70 (93%)	
	9.96 ± 1.57 (7%)	0.35 ± 0.11
YtvA-N104S	3.0 ± 0.2	0.4 ± 0.06
YtvA-Q123N	1.6 ± 0.14	0.22 ± 0.03

[a] The errors derive from two independent measurements (three for YtvA-N104D). [b] This value is probably underestimated due to partial chromophore detachment from the protein.

with triplet formation are poorly affected by the mutations. This latter parameter is solely strongly reduced in YtvA-N104A, for which also the value of Φ_T is slightly smaller. Thus, together with N104S, N104A is the only substitution, among those investigated, that affects triplet formation.

Temperature Dependence of the Recovery Kinetics. As for the recovery lifetimes, τ_{rec}, all mutations affect to some extent the kinetics as measured at 20 °C and/or the activation energy or the pre-exponential factor as derived from Arrhenius or Eyring plots (eqs 5a and 5b, respectively), where k_B and R are the Boltzmann and gas constants, respectively, and h is the Planck's constant.[71]

$$\ln \frac{1}{\tau_{rec}} = \ln A - \frac{E_a}{R}\frac{1}{T} \quad (5a)$$

$$\ln \frac{1}{\tau_{rec} T} = \ln \frac{k_B}{h} + \frac{\Delta S^{\#}}{R} - \frac{\Delta H^{\#}}{R}\frac{1}{T} \quad (5b)$$

Major changes are observed for (i) Q123N, with a dramatic fastening of the photocycle, correlated to a lowering of E_a, i.e., of $\Delta H^{\#}$ (activation enthalpy change), and furthermore the decay is clearly bi-exponential for this protein (the weighted average value is reported in Table 5), and for (ii) N94A and N94S, with a significant acceleration of the photocycle, but in this case it is

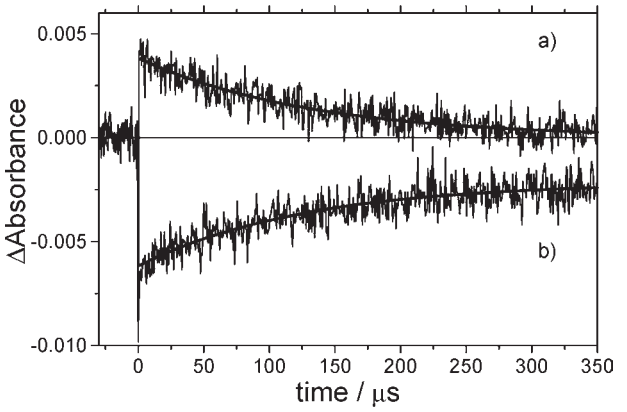

Figure 4. (a) Triplet decay (detection at 650 nm) and (b) photoproduct formation (detection at 450 nm, corresponding to the bleaching of the parent state) for YtvA-N94A. The curves derived from a monoexponential fitting decay function of the flash photolysis signals (excitation at 450 nm) are overlaid with the experimental traces. The two processes are synchronous, with recovered lifetimes τ_T of 129 and 126 μs, respectively; these kinetics are more than 60 times slower than for YtvA-WT, for which τ_T = 2 μs (see Table 2).

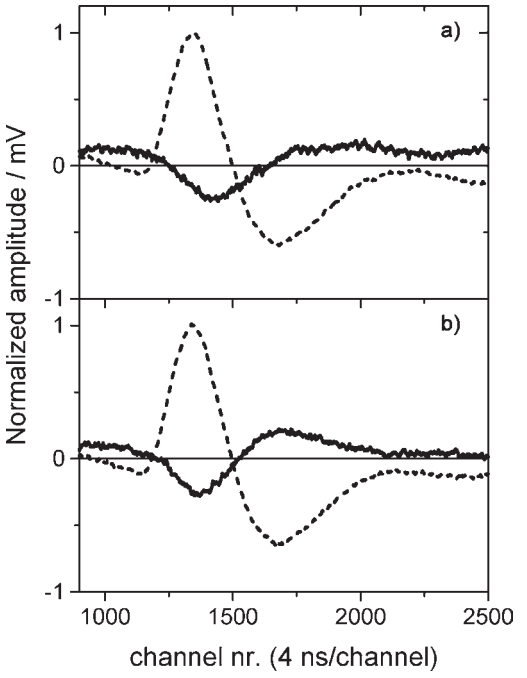

Figure 5. LIOAS signals (solid lines) for (a) YtvA-N104D and (b) YtvA-Q123N, showing light-induced structural changes (ΔV_i) as detected at $T_{\beta=0}$ = 3.2 °C. The reference curves (dotted lines), with normalized maximal amplitude = 1, are recorded at $T_{\beta>0}$ = 10 °C. Notice that the ΔV_i pattern extends to a longer time scale in YtvA-N104D (which behaves similarly to YtvA-WT[59]); i.e., it bears contributions both from triplet formation (ΔV_1, τ_1 < 20 ns) and from triplet decay/adduct formation (ΔV_2, $\tau_2 \approx$ 1.3 μs). The second volume change component is absent in YtvA-Q123N, although the adduct is formed on the same time scale as YtvA-WT (see Tables 3 and 4 for the detailed results of deconvolution).

correlated to an increase of the Arrhenius pre-exponential factor, i.e., an increase of $\Delta S^{\#}$ (activation entropy change). In N94D the increase in $\Delta S^{\#}$ more than compensates for the concomitant increase in $\Delta H^{\#}$, thus resulting in a faster photocycle at 20 °C,

dx.doi.org/10.1021/ja1097379 |J. Am. Chem. Soc. 2011, 133, 5346–5356

Table 3. Parameters Derived from Deconvolution of LIOAS Signals

	α_1 (τ_1 < 20 ns)	α_2	τ_2/μs	ΔV_1/mL einstein^{-1}	ΔV_2/mL einstein^{-1}
YtvA-WT[a]	0.30 ± 0.03	0.23 ± 0.04	1.90 ± 0.21	−0.44 ± 0.05	−5.8 ± 0.2
YtvA-N94D	0.38 ± 0.01	0.16 ± 0.03	1.2 ± 0.30	−0.66 ± 0.03	−2.36 ± 0.22
YtvA-N94A	0.29 ± 0.02		>5	−0.50 ± 0.01	
YtvA-N94S	0.41 ± 0.02	0.16 ± 0.05	1.96 ± 0.22	−0.93 ± 0.08	−0.6 ± 0.3
YtvA-N104D	0.26 ± 0.03	0.32 ± 0.05	1.36 ± 0.2	−0.75 ± 0.18	−3.2 ± 0.2
YtvA-N104A	0.41 ± 0.03	0.14 ± 0.03	1.95 ± 0.60	−0.05 ± 0.03	−3.5 ± 0.2
YtvA-N104S	0.18 ± 0.03	0.28 ± 0.07	2.47 ± 0.79	−0.84 ± 0.17	−4.11 ± 0.26
YtvA-Q123N	0.31 ± 0.02	0.20 ± 0.01	1.16 ± 0.10	−1.70 ± 0.08	

[a] From ref 59. The errors are from two independent signals and four deconvolutions.

Table 4. Triplet Yield, Energy Storage, and Structural Changes in Mutated YtvA Proteins

	Φ_T[a]	$E_{390}\Phi_{390}$/kJ mol^{-1}[b]	E_{390}/kJ mol^{-1}[c]	ΔV_{660}/mL mol^{-1}[d]	ΔV_{390}/mL mol^{-1}[e]
YtvA-WT	0.62 ± 0.03	67 ± 9	137 ± 19	−0.70 ± 0.07	−12.60 ± 0.80
YtvA-N94D	0.59 ± 0.01	76 ± 10	ND[f]	−1.10 ± 0.05	ND[f]
YtvA-N94A	0.56 ± 0.02			−0.89 ± 0.03	
YtvA-N94S	0.56 ± 0.03	69 ± 15	131 ± 40	−1.66 ± 0.15	−2.90 ± 0.60
YtvA-N104D	0.64 ± 0.04	43 ± 18	133 ± 107	−1.18 ± 0.25	−11.10 ± 5.90
YtvA-N104A	0.47 ± 0.04	57 ± 9	175 ± 56	−0.11 ± 0.05	−10.80 ± 2.70
YtvA-N104S	0.79 ± 0.03	84 ± 18	213 ± 49	−1.06 ± 0.19	−11.50 ± 1.30
YtvA-Q123N	0.50 ± 0.03	48 ± 4	224 ± 30	−3.40 ± 0.20	−3.40 ± 0.20

[a] Equation 3a. [b] Equation 3b. [c] Using Φ_{390} values and the associated errors from Table 2. [d] Equation 4a, using Φ_T from this table and ΔV_1 from Table 3, with associated errors. [e] Equation 4b, using Φ_{390} from Table 2 and ΔV_2 from Table 3, with associated errors. [f] ND = not determined. The underestimation of Φ_{390} in Table 2, due to protein instability, would give for E_{390} a value of 345 kJ/mol; this value is larger than the excitation photon energy of 265.8 kJ/mol.

Table 5. Recovery Kinetics (20 °C) and Arrhenius and Eyring Parameters

	$\tau_{rec,20}$/s	A/s^{-1}	E_a/kJ mol^{-1}	$\Delta H^{\#}$/kJ mol^{-1}	$\Delta S^{\#}$/kJ mol^{-1} K^{-1}
YtvA-WT	6240	6.9×10^{14}	104	101	+0.031
YtvA-N94D	1250	3.4×10^{23}	151	148	+0.20
YtvA-N94A	140	4.9×10^{18}	117	115	+0.10
YtvA-N94S	300	7.2×10^{15}	103	100	+0.05
YtvA-N104D	6890	4.9×10^{16}	115	112	+0.066
YtvA-N104A	2250	4.0×10^{8}	67	65	−0.09
YtvA-N104S	1120	9.2×10^{10}	78	76	−0.043
YtvA-Q123N	72	5.0×10^{9}	65	62	−0.067

albeit not so dramatic as in N94A and N94S. Mutations of N104 (see Figure 1 for the HB network centered on this residue) result in less profound effects on the overall kinetics of the photocycle, but they still considerably lower the activation energy (N/A and N/S changes).

DISCUSSION

Switching Glutamine on Strand Iβ and N(5) of the Flavin Ring. The strong acceleration of the photocycle in YtvA-Q123N, which recovers with a τ_{rec} about 85 times faster than YtvA-WT (at 20 °C), parallels the 1.8 times acceleration observed for the corresponding Q513N mutation in *As*phot1-LOV2,[50] although for YtvA the effect is significantly more pronounced. We can therefore safely state that this substitution destabilizes the covalent adduct. This is reflected in the high energy content of the photoadduct for YtvA-Q123N (Table 4) and in the lowering of the activation energy for the recovery reaction (Table 5, Figure 6), accounting for the fast photocycle at room temperature. The decay of the adduct, clearly bi-exponential in this mutated protein, also points to a conformational heterogeneity in the light-activated state. Interestingly, Alexandre and co-workers detected a mixed one-/two-HB arrangement at C(4)═O in the dark state of *As*phot-LOV2, indicative of a conformational flexibility in this protein region.[8] The asparagine substitution could enhance this flexibility, which becomes clearly evident in the double-exponential decay. This mutation also affects the forward photochemistry, although to a minor extent, by accelerating the triplet decay and lowering the quantum yield of the photocycle (Table 2). These latter effects, together with the subtle shifts observed in absorption and fluorescence, point to a limited but well detectable role of the direct HB partner of N(5)

dx.doi.org/10.1021/ja1097379 |*J. Am. Chem. Soc.* 2011, 133, 5346–5356

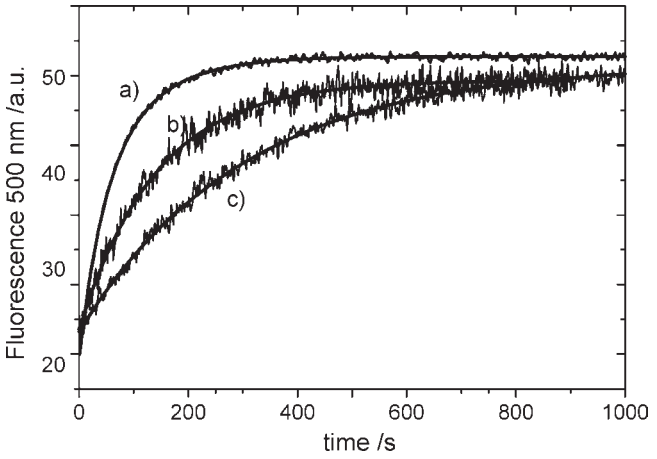

Figure 6. Recovery kinetics of fast-cycling mutated YtvA proteins at 20 °C, monitored via the growing fluorescence of FMN at 500 nm (excitation at 303 nm). Interpolated lines, as obtained by exponential fitting, are superimposed on the experimental curves. (a) YtvA-Q123N (showing biexponential kinetics), τ_{rec1}= 44 s (51%) and τ_{rec2} = 102 s (49%); (b) YtvA-N94A, τ_{rec}= 140 s; (c) YtvA-N94S, τ_{rec}= 300 s (Table 5).

in the light state in determining the efficiency of the photochemical step in LOV domains. In addition, the much more substantial role that this residue plays in the later steps of the photocycle and during the molecular events underlying signal propagation has to be kept in mind. In *As*phot1-LOV2, the molecular event crucial for activation of the C-terminal kinase domain is the light-triggered unfolding of the Jα helical linker, otherwise organized underneath the LOV2 β-scaffold in the dark state.[13,72] In these investigations, LOV2-Q513N is conformationally locked in a pseudo-lit state, i.e., the linker is not helical in the dark, whereas Q513L is locked in a pseudo-dark state, i.e., there is no light-triggered unfolding of the linker.[50] These observations are fully compatible with the general proposed role for this conserved glutamine to act as a conformational switch in LOV domains.[32,51,53] This suggestion is well supported by our results that reveal the lack of structural changes in Q123N during the formation of the adduct (Tables 3 and 4). Only in few cases has the link between reduced or suppressed conformational changes and functional effects been established, e.g., in *At*phot1, where the Q575L mutation on LOV2 diminishes light-driven conformational changes[53] and attenuates light-induced self-phosphorylation.[55] Most important for our work is the finding of the physiological effect for this YtvA mutation (Q123N), which suppresses the light-dependent upregulation of the alternative transcription factor σ^{B},[54] thus complementing our photophysical data.

Hydrogen-Bond Network Builder Asparagines N94 and N104: Tuning the Photocycle. Besides their obvious role in stabilizing the polar part of the isoalloxazine ring via the formation of hydrogen bonds to C(2)═O, N(3)H, and C(4)═O within the protein cavity, the two conserved asparagines seem to play a major role in determining the kinetics of the photocycle, including the formation of the adduct, by building an optimal HB network. Mutation of these polar residues into aspartates in principle is not innocent, in that we most probably introduce a negative charge within the protein cavity that requires a rearrangement of the HB network shown in Figure 1. We note that N94D induces a red-shift in the UVA absorption band, a phenomenon that, for free flavins, has been correlated with the presence of proton-donating solvents.[47] The red-shift of transition II, observed only for N94D and not for N104D, confirms that the transition dipole is oriented toward C(2)═O, as previously proposed (see Figure 2 for the transition dipole orientation of this band).[41,42] The data could indicate that the aspartate in position 94 is protonated or shares its proton such that the hydroxy group interacts with C(2)═O as a donor in the HB. However, we note that a similar red-shift of the UVA band is observed for *As*phot1-LOV2 with respect to LOV1,[69] for which NMR analysis has suggested a weaker HB to C(2)═O.[45]

Transition I undergoes a slight blue-shift for both mutations, larger for N104D (4 nm) than for N94D (2 nm). This could be well explained by a geometric effect such that the HB formed by the lateral chain of aspartic acid with the C(4)═O/N(3)H groups on FMN is extended in length or even is lost. Yet, residue N94 might also be partly involved in these effects in supporting the ring geometry to be re-adjusted to the introduced carboxylate moiety (N104D). A slight hypsochromic shift is observed for this band in LOV2 with respect to LOV1,[69] for which HB at C(4)═O and C(2)═O is stronger.[45] Furthermore, *As*phot1-LOV2 exists in an equilibrium of singly and doubly H-bonded C(4)═O conformers in the dark state, in which the stronger (double-bonded) HB induces a red-shift of this band.[8] Therefore, we can suggest that, in YtvA-Q123N, YtvA-N104D, and, to a lesser extent, YtvA-N94D, the HB at C(4)═O is weaker than in YtvA-WT, and this feature induces a moderate acceleration of triplet decay/adduct formation. Nevertheless, the effects of aspartic acid might be due instead to the presence of a negative charge within the cavity, due to the low pK_a (ca. 4) of the lateral chain in this residue. Due to instability of the protein at low pH, we were not able to determine the pK_a of D94 and D104, but we note that, as for the energy of the electronic transitions, the introduction of aspartic acid in position 94 or 104 is more perturbing than introducing residues such as serine or alanine that conceivably suppress local HB with the chromophore (Table 1). The latter mutations have instead a more pronounced effect on the photochemical reactions, ranging from an increase of triplet quantum yield in YtvA-N104S to a slowing-down of triplet decay into the adduct, which becomes dramatic in YtvA-N94A. In the latter mutant, photoadduct formation is 65-fold slower than for YtvA-WT (see Table 2), counteracted by a 44-fold faster recovery kinetics. This large effect on the forward kinetics is not accompanied by a concomitant decrease of the photocycle quantum yield, indicating that possible competitive processes, e.g., quenching from molecular oxygen, have a negligible yield.

Recovery Reaction and the Link between Chromophore–Protein Interactions and Signal Propagation. From Table 5, the increase in the rate of the recovery reaction due to the substitution of the "flipping" glutamine Q123[7] appears to be related to a more favorable activation enthalpy, i.e., a value lower than for YtvA-WT. Concomitantly, the LIOAS data indicate a high energy level for the photoadduct in YtvA-Q123N, which might be responsible for lowering the energy barrier for the recovery reaction. These results, together with the lack of structural changes concomitant with this step (Tables 3 and 4), suggest that the light-induced flipping does not occur in this mutated protein and that this missing "switch" could be responsible for the observed *in vivo* effects, where YtvA-Q123N does not show any light-induced activity.[54] A similar effect on the activation parameters is observed for N104A/S mutations that conceivably

disrupt the HB network centered on C(4)═O, thus also influencing the effect of Q123 (Figure 1). We note that N104 is adjacent to E105, a residue functionally essential for inter-domain signal transmission in YtvA[52] and for its *in vivo* light-induced effects.[54] Therefore, this chromophore region, with its HB partner amino acids, could represent the link between light activation, photocycle duration, and signal propagation from the FMN binding pocket to the surface of the LOV core, thereby confirming and extending the proposed key role of the "switching glutamine".[50,51,53]

In contrast, suppression of the extended HB network centered at N94 (N94S and N94A) and involving C(2)═O/N(3)H still results in an accelerated photocycle at 20 °C, but in this case the activation parameters point to a more favorable entropic term that is larger than for YtvA-WT. This indicates that the rearrangement of this HB network is one of the rate-limiting steps on the way back to the dark state, besides being a major determinant for triplet formation and decay (*vide supra*). We are instead not aware of any link between the protein region containing N94, localized on strand Gβ, and signal propagation. Strand Gβ residues are not part of the LOV−LOV interface in the crystal structure[7] and in the structural model[52] of YtvA−LOV. One putative mechanism could rely on the adjacent conserved salt bridge formed by E56 (on Dα) and K97 (Gβ-Hβ loop), linked to the inner FMN cavity via a conserved arrangement of several amino acids.[73] Molecular dynamics (MD) simulations have suggested that light-induced strengthening of the E−K salt bridge is a characteristics of LOV1 which thereby becomes less mobile in the light state.[74] In LOV2, instead, the E−K salt bridge should be stable in both dark and light states, with conformational changes occurring mainly within the Hβ−Iβ loop and the adjacent regions of the central β-sheet that becomes more mobile.[74] Freddolino et al. have suggested that these changes are initiated in LOV1 by the asparagines corresponding to N104 in YtvA, thus solely indirectly involving N94, whereas LOV2 activation should be mediated by Q123.[74] Accordingly, mutation of the E−K in LOV2 does not affect light-driven self-phosphorylation of phot1.[55] There is, however, up to now no experimental evidence in favor of the MD simulations of the activation mechanism of LOV1, given that we still are missing a readout response for LOV1 functional activity. In any case, these two proposed different activation mechanisms between LOV1 and LOV2 should both be triggered by modifications of the HB around FMN.

Relevance for the Mechanism of Adduct Formation and Decay. High-resolution FTIR techniques have recently provided evidence that the triplet state of FMN bound to LOV domains is unprotonated,[31,32] thus disfavoring a previously proposed ionic mechanism.[75] According to the latter, the increase in pK_a of N(5) in the triplet state should trigger its protonation, leaving a single HN(5)−C(4a) bond that can be easily attacked by the thiolate of the cysteine.[75] The radical pair mechanism predicts the formation of a triplet-state $FMNH^{\bullet}-H_2CS^{\bullet}$ biradical, where a rapid triplet−singlet conversion is induced by the sulfur atom, followed by radical-pair recombination between $H_2CS^{\bullet}$ and the unpaired electron on C(4a).[76,77] Recently it was suggested that the first FMN radical species formed might be the negatively charged semiquinone $FMN^{\bullet-}$.[33] During the revision of this manuscript, the first direct evidence of an intermediate species between the triplet state and the adduct, by means of nanosecond flash photolysis with CCD camera detection and a special flow cell design, was reported.[78] The new transient species is spectrally similar to a neutral flavin radical, and it is suggested to decay fast into the adduct.[78]

The time resolution and the molecular details provided by the techniques employed in this work are certainly not suitable to detect the putative radical intermediates, but we can observe that the introduction of probably negatively charged aspartates in the cavity has no dramatic effect on the dynamics and energetics of adduct formation (Tables 2 and 4). This would probably be the case if transiently charged species (e.g., in the ionic mechanism) were present. Our data seem thus to agree with the occurrence of a neutral flavin radical.[78] The extremely slow decay of the flavin triplet in N94A suggests that polarity/polarizability effects must be operating during formation of the adduct, indeed pointing to a strong electronic rearrangement, which is not in contrast with the radical-pair hypothesis. High-resolution FTIR techniques applied to this mutated protein could provide useful information on the mechanism of adduct formation.

Modulation of the photocycle by altering the HB network at the flavin ring complements previous data suggesting that the microenvironment around N(5) is a major determinant for the dark recovery reaction, in particular suggested by pH effects, base catalysis, and mutations at position Q123.[28,29,50] Other mutations are able to affect the photocycle kinetics by altering steric restrictions or the HB network that stabilizes the ribityl chain.[2,3,27,29,34,38,50] To our knowledge, we have here, for the first time, highlighted the role played by the asparagine residues directly H-bonded to C(4)═O and C(2)═O, namely at polar sites on the isoalloxazine ring that determine chromophore spectral properties and photoreactivity.

Hydrogen-Bond Network as a Tool To Modulate the Photocycle: Relevance for Optogenetics Applications. BL receptors of the LOV and BLUF families are increasingly employed as photofunctional proteins in the growing field of optogenetics, a research field prompted by the possibility of regulating cellular machinery with optimal spatial and temporal control.[11,12,34,35,37,79,82] The lifetime of the photoactivated state is of primary importance, in that it determines the duration of the cellular response of interest and has to be tuned to meet the particular metabolic characteristics of a given cell.[37] Mutations of amino acids in the vicinity of the flavin chromophore, such as those we have presented here, can be readily exploited to achieve a given photocycle kinetics. The only condition required is the intactness of the light-to-signal transduction, namely the fact that the protein must remain functionally active, a condition that might not be met in certain instances, e.g., upon mutation of the flipping glutamine (*vide supra*).

Hydrogen-Bond Network as a Possible Redox Potential Regulator? While this article was under review, novel data on the midpoint potential of FAD bound to a BLUF domain were reported, suggesting that the HB network around the flavin chromophore might modulate both the absorption maximum and the midpoint potential of BL photoreceptors.[83] Those authors determined the values of both parameters for WT and mutated BLUF domains of the protein AppA (referred to as $AppA_{1-125}$), and for two LOV proteins. The values are as follows (absorption maximum/midpoint potential): $AppA_{1-125}$, 448 nm/−255 mV; $AppA_{1-125}$Q63N, 446 nm/−260 mV; $AppA_{1-125}$Y21F, 444 nm/−260 mV; $AppA_{1-125}$W104A, 444 nm/−260 mV; $AppA_{1-125}$Q63H, 441 nm/−230 mV $AppA_{1-125}$Y21FW104F, 442 nm/−217 mV; YtvA, 449 nm/−308 mV; Asphot1-LOV2, 448 nm/−307 mV.[83] The correlation between absorption maxima and midpoint potential is rather

dx.doi.org/10.1021/ja1097379 |*J. Am. Chem. Soc.* 2011, 133, 5346–5356

vague and certainly needs to be better substantiated within the LOV series, in view of a potential integration of light and redox signals within the cell. Such integration has been shown to be possible for the LOV kinase (LOVK) from *C. crescentus*, for which the midpoint potential of −258 mV has been determined, a value very similar to AppA, and in the same range as the proposed redox potential of a bacterial cell (−260 to −280 mV).[84] The absorption maximum of LOVK lies indeed at 446 nm, as for AppA.[83,84] Interestingly, the midpoint potential changes to −303 mV if the LOV core alone of LOVK (aa 1−138) is investigated; this truncation does not alter the absorption maximum, indicating that structural aspects seem also to be important in determining the midpoint potential.[84]

This subject is certainly intriguing, and some of the mutated YtvA proteins discussed here, in particular those able to shift the absorption maximum, are good candidates to test the possible interrelation between transition energy and redox potential in LOV proteins.

CONCLUSIONS

Modifications of the conserved HB network that stabilizes the isoalloxazine ring within a LOV domain, affects the photocycle kinetics, both for formation and decay of the signaling state. A major contribution is provided by the glutamine residue interacting with N(5) in the light-activated state, a position that becomes protonated, thus causing a flipping of the amino acid side chain and being identified as a major event during signal transmission to the LOV domain surface. A second key element is the extended HB network centered on N94: suppression of the network by the Asn/Ala mutation dramatically slows down the photochemical reaction and accelerates the decay of the photoadduct. The intactness of the HB network thus appears to be essential for the optimization of the photocycle, most probably by tuning it to the velocity and efficiency of signal-transduction events and, ultimately, of functional and *in vivo* responses.

ASSOCIATED CONTENT

Supporting Information. Details of primer design and sequences used in this work for site-directed mutagenesis. This material is available free of charge via the Internet at http://pubs.acs.org.

AUTHOR INFORMATION

Corresponding Author
aba.losi@fis.unipr.it

ACKNOWLEDGMENT

This work has been partially supported by the Deutsche Forschungsgemeinschaft (FOR526). We thank Sarah Klassen for her valuable help in the laboratory. The LIOAS equipment and the laser system employed in this work were kindly donated by the Max-Planck-Institute for Bioinorganic Chemistry (Muelhim and der Ruhr, Germany) to the University of Parma.

REFERENCES

(1) Losi, A. *Photochem. Photobiol.* **2007**, *83*, 1283–1300.
(2) Christie, J. M.; Corchnoy, S. B.; Swartz, T. E.; Hokenson, M.; Han, I. S.; Briggs, W. R.; Bogomolni, R. A. *Biochemistry* **2007**, *46*, 9310–9319.
(3) Brosi, R.; Illarionov, B.; Mathes, T.; Fischer, M.; Joshi, M.; Bacher, A.; Hegemann, P.; Bittl, R.; Weber, S.; Schleicher, E. *J. Am. Chem. Soc.* **2010**, *132*, 8935–8944.
(4) Crosson, S.; Moffat, K. *Plant Cell* **2002**, *14*, 1067–1075.
(5) Fedorov, R.; Schlichting, I.; Hartmann, E.; Domratcheva, T.; Fuhrmann, M.; Hegemann, P. *Biophys. J.* **2003**, *84*, 2492–2501.
(6) Iwata, T.; Nozaki, D.; Tokutomi, S.; Kagawa, T.; Wada, M.; Kandori, H. *Biochemistry* **2003**, *42*, 8183–8191.
(7) Möglich, A.; Moffat, K. *J. Mol. Biol.* **2007**, *373*, 112–126.
(8) Alexandre, M. T. A.; van Grondelle, R.; Hellingwerf, K. J.; Kennis, J. T. M. *Biophys. J.* **2009**, *97*, 238–247.
(9) Christie, J. M. *Annu. Rev. Plant Biol.* **2007**, *58*, 21–45.
(10) Halavaty, A. S.; Moffat, K. *Biochemistry* **2007**, *46*, 14001–14009.
(11) Möglich, A.; Yang, X. J.; Ayers, R. A.; Moffat, K. *Annu. Rev. Plant. Phys.* **2010**, 21–47.
(12) Möglich, A.; Ayers, R. A.; Moffat, K. *Structure* **2009**, *17*, 1282–1294.
(13) Harper, S. M.; Neil, L. C.; Gardner, K. H. *Science* **2003**, *301*, 1541–1544.
(14) Schwerdtfeger, C.; Linden, H. *EMBO J.* **2003**, *22*, 4846–4855.
(15) Briggs, W. R.; Tseng, T. S.; Cho, H. Y.; Swartz, T. E.; Sullivan, S.; Bogomolni, R. A.; Kaiserli, E.; Christie, J. M. *J. Integr. Plant Biol.* **2007**, *49*, 4–10.
(16) Losi, A.; Gärtner, W. *Photochem. Photobiol. Sci.* **2008**, *7*, 1168–1178.
(17) Krauss, U.; Minh, B. Q.; Losi, A.; Gärtner, W.; Eggert, T.; von Haeseler, A.; Jaeger, K.-E. *J. Bacteriol.* **2009**, *191*, 7234–7242.
(18) Pathak, G.; Ehrenreich, A.; Losi, A.; Streit, W. R.; Gärtner, W. *Environ. Microbiol.* **2009**, *11*, 2388–2399.
(19) Swartz, T. E.; Corchnoy, S. B.; Christie, J. M.; Lewis, J. W.; Szundi, I.; Briggs, W. R.; Bogomolni, R. A. *J. Biol. Chem.* **2001**, *276*, 36493–36500.
(20) Purcell, E. B.; Siegal-Gaskins, D.; Rawling, D. C.; Fiebig, A.; Crosson, S. *Proc. Natl. Acad. Sci. U.S.A.* **2007**, *104*, 18241–18246.
(21) Idnurm, A.; Crosson, S. *PLoS Pathogens* **2009**, *5*, e1000470.
(22) Swartz, T. E.; Corchnoy, S. B.; Christie, J. M.; Lewis, J. W.; Szundi, I.; Briggs, W. R.; Bogomolni, R. A. *J. Biol. Chem.* **2001**, *276*, 36493–36500.
(23) Kottke, T.; Heberle, J.; Hehn, D.; Dick, B.; Hegemann, P. *Biophys. J.* **2003**, *84*, 1192–1201.
(24) Kasahara, M.; Swartz, T. E.; Olney, M. A.; Onodera, A.; Mochizuki, N.; Fukuzawa, H.; Asamizu, E.; Tabata, S.; Kanegae, H.; Takano, M.; Christie, J. M.; Nagatani, A.; Briggs, W. R. *Plant Physiol.* **2002**, *129*, 762–773.
(25) Nakasako, M.; Matsuoka, D.; Zikihara, K.; Tokutomi, S. *FEBS Lett.* **2005**, *579*, 1067–1071.
(26) Kikuchi, S.; Unno, M.; Zikihara, K.; Tokutomi, S.; Yamauchi, S. *J. Phys. Chem. B* **2009**, *113*, 2913–2921.
(27) Jentzsch, K.; Wirtz, A.; Circolone, F.; Drepper, T.; Losi, A.; Gärtner, W.; Jaeger, K.-E.; Krauss, U. *Biochemistry* **2009**, *48*, 10321–10333.
(28) Alexandre, M. T. A.; Arents, J. C.; van Grondelle, R.; Hellingwerf, K. J.; Kennis, J. T. M. *Biochemistry* **2007**, *46*, 3129–3137.
(29) Zoltowski, B. D.; Vaccaro, B.; Crane, B. R. *Nat. Chem. Biol.* **2009**, *5*, 827–834.
(30) Corchnoy, S. B.; Swartz, T. E.; Lewis, J. W.; Szundi, I.; Briggs, W. R.; Bogomolni, R. A. *J. Biol. Chem.* **2003**, *278*, 724–731.
(31) Alexandre, M. T. A.; Domratcheva, T.; Bonetti, C.; van Wilderen, L. J. G. W.; van Grondelle, R.; Groot, M. L.; Hellingwerf, K. J.; Kennis, J. T. M. *Biophys. J.* **2009**, *97*, 227–237.
(32) Pfeifer, A.; Majerus, T.; Zikihara, K.; Matsuoka, D.; Tokutomi, S.; Heberle, J.; Kottke, T. *Biophys. J.* **2009**, *96*, 1462–1470.
(33) Lanzl, K.; Sanden-Flohe, M. V.; Kutta, R. J.; Dick, B. *Phys. Chem. Chem. Phys.* **2010**, *12*, 6594–6604.
(34) Möglich, A.; Moffat, K. *Photochem. Photobiol. Sci.* **2010**, *9*, 1286–1300.
(35) Zoltowski, B. D.; Gardner, K. H. *Biochemistry* **2011**, *50*, 4–16.
(36) Ryu, M. H.; Moskvin, O. V.; Siltberg-Liberles, J.; Gomelsky, M. *J. Biol. Chem.* **2010**, *285*, 41501–41508.

(37) Stierl, M.; Stumpf, P.; Udwari, D.; Gueta, R.; Hagedorn, R.; Losi, A.; Gärtner, W.; Petereit, L.; Efetova, M.; Schwarzel, M.; Oertner, T. G.; Nagel, G.; Hegemann, P. *J. Biol. Chem.* **2011**, *286*, 1181–1188.
(38) Losi, A.; Kottke, T.; Hegemann, P. *Biophys. J.* **2004**, *86*, 1051–1060.
(39) Tang, Y.; Cao, Z.; Livoti, E.; Krauss, U.; Jaeger, K.-E.; Gärtner, W.; Losi, A. *Photochem. Photobiol. Sci.* **2010**, *9*, 47–56.
(40) Mansurova, M.; Scheercousse, P.; Simon, J.; Kluth, M.; Gärtner, W. *ChemBioChem* **2011**, *12*, 641–646.
(41) Climent, T.; Gonzalez-Luque, R.; Merchan, M.; Serrano-Andres, L. *J. Phys. Chem. A* **2006**, *110*, 13584–13590.
(42) Johansson, L. B.; Davidsson, A.; Lindblom, G.; Naqvi, K. R. *Biochemistry* **1979**, *18*, 4249–4253.
(43) Nozaki, D.; Iwata, T.; Ishikawa, T.; Todo, T.; Tokutomi, S.; Kandori, H. *Biochemistry* **2004**, *43*, 8373–8379.
(44) Iwata, T.; Nozaki, D.; Sato, Y.; Sato, K.; Nishina, Y.; Shiga, K.; Tokutomi, S.; Kandori, H. *Biochemistry* **2006**, *45*, 15384–15391.
(45) Eisenreich, W.; Joshi, M.; Illarionov, B.; Richter, G.; Römisch-Margl, W.; Müller, F.; Bacher, A.; Fischer, M. *FEBS J.* **2007**, *274*, 5876–5890.
(46) Alexandre, M. T. A.; Purcell, E. B.; van Grondelle, R.; Robert, B.; Kennis, J. T. M.; Crosson, S. *Biochemistry* **2010**, *49*, 4752–4759.
(47) Kotaki, A.; Naoi, M.; Yagi, K. *J. Biochem.* **1970**, *68*, 287–292.
(48) Yagi, K.; Ohishi, N.; Nishimoto, K.; Choi, J. D.; Song, P. S. *Biochemistry* **1980**, *19*, 1553–1557.
(49) Salzmann, S.; Silva-Junior, M. R.; Thiel, W.; Marian, C. M. *J. Phys. Chem. B* **2009**, *113*, 15610–15618.
(50) Nash, A. I.; Ko, W. H.; Harper, S. M.; Gardner, K. H. *Biochemistry* **2008**, *47*, 13842–13849.
(51) Zoltowski, B. D.; Schwerdtfeger, C.; Widom, J.; Loros, J. J.; Bilwes, A. M.; Dunlap, J. C.; Crane, B. R. *Science* **2007**, *316*, 1054–1057.
(52) Buttani, V.; Losi, A.; Eggert, T.; Krauss, U.; Jaeger, K.-E.; Cao, Z.; Gärtner, W. *Photochem. Photobiol. Sci.* **2007**, *6*, 41–49.
(53) Yamamoto, A.; Iwata, T.; Sato, Y.; Matsuoka, D.; Tokutomi, S.; Kandori, H. *Biophys. J.* **2009**, *96*, 2771–2778.
(54) Avila-Perez, M.; Vreede, J.; Tang, Y.; Bende, O.; Losi, A.; Gärtner, W.; Hellingwerf, K. *J. Biol. Chem.* **2009**, *284*, 24958–24964.
(55) Jones, M. A.; Feeney, K. A.; Kelly, S. M.; Christie, J. M. *J. Biol. Chem.* **2007**, *282*, 6405–6414.
(56) Lapid, C. *PrimerX*, Automated design of mutagenic primers for site-directed mutagenesis; 2003; http://www.bioinformatics.org/primerx/.
(57) Losi, A.; Polverini, E.; Quest, B.; Gärtner, W. *Biophys. J.* **2002**, *82*, 2627–2634.
(58) Losi, A.; Wegener, A. A.; Engelhard, M.; Gärtner, W.; Braslavsky, S. E. *Biophys. J.* **2000**, *78*, 2581–2589.
(59) Losi, A.; Quest, B.; Gärtner, W. *Photochem. Photobiol. Sci.* **2003**, *2*, 759–766.
(60) Rudzki, J. E.; Goodman, J. L.; Peters, K. S. *J. Am. Chem. Soc.* **1985**, *107*, 7849–7854.
(61) Abbruzzetti, S.; Viappiani, C.; Murgida, D. H.; Erra-Balsells, R.; Bilmes, G. M. *Chem. Phys. Lett.* **1999**, *304*, 167–172.
(62) Braslavsky, S. E.; Heibel, G. E. *Chem. Rev.* **1992**, *92*, 1381–1410.
(63) Rudzki-Small, J.; Libertini, L. J.; Small, E. W. *Biophys. Chem.* **1992**, *41*, 29–48.
(64) Malkin, S.; Churio, M. S.; Shochat, S.; Braslavsky, S. E. *J. Photochem. Photobiol. B: Biol.* **1994**, *23*, 79–85.
(65) Losi, A.; Braslavsky, S. E. *Phys. Chem. Chem. Phys.* **2003**, *5*, 2739–2750.
(66) Gauden, M.; Crosson, S.; van Stokkum, I. H. M.; van Grondelle, R.; Moffat, K.; Kennis, J. T. M. . In *Femtosecond Laser Applications in Biology*; Avrilleir, S., Tualle, J. M., Eds.; SPIE: Bellingham, WA, 2004; pp 97−104.
(67) Van den Berg, P. W.; Widengren, J.; Hink, M. A.; Rigler, R.; Visser, A. G. *Spectrochim. Acta A* **2001**, *57*, 2135–2144.
(68) Zirak, P.; Penzkofer, A.; Mathes, T.; Hegemann, P. *Chem. Phys.* **2009**, *358*, 111–122.
(69) Salomon, M.; Christie, J. M.; Knieb, E.; Lempert, U.; Briggs, W. R. *Biochemistry* **2000**, *39*, 9401–9410.
(70) Philip, A. F.; Nome, R. A.; Papadantonakis, G. A.; Scherer, N. F.; Hoff, W. D. *Proc. Natl. Acad. Sci. U.S.A.* **2010**, *107*, 5821–5826.
(71) Winzor, D. J.; Jackson, C. M. *J. Mol. Recognit.* **2006**, *19*, 389–407.
(72) Harper, S. M.; Christie, J. M.; Gardner, K. H. *Biochemistry* **2004**, *43*, 16184–16192.
(73) Crosson, S.; Rajagopal, S.; Moffat, K. *Biochemistry* **2003**, *42*, 2–10.
(74) Freddolino, P. L.; Dittrich, M.; Schulten, K. *Biophys. J.* **2006**, *91*, 3630–3639.
(75) Corchnoy, S. B.; Swartz, T. E.; Szundi, I.; Lewis, J. W.; Briggs, W. R.; Bogomolni, R. A. *Biophys. J.* **2003**, *84*, 398A.
(76) Schleicher, E.; Kowalczyk, R. M.; Kay, C. W. M.; Hegemann, P.; Bacher, A.; Fischer, M.; Bittl, R.; Richter, G.; Weber, S. *J. Am. Chem. Soc.* **2004**, *126*, 11067–11076.
(77) Bonetti, C.; Stierl, M.; Mathes, T.; van Stokkum, I. H. M.; Mullen, K. M.; Cohen-Stuart, T. A.; van Grondelle, R.; Hegemann, P.; Kennis, J. T. M. *Biochemistry* **2009**, *48*, 11458–11469.
(78) Bauer, C.; Rabl, C. R.; Heberle, J.; Kottke, T. *Photochem. Photobiol.* **2011**No. DOI: 10.1111/j.1751-1097.2011.00901.x.
(79) Nagahama, T.; Suzuki, T.; Yoshikawa, S.; Iseki, M. *Neurosci. Res.* **2007**, *59*, 81–88.
(80) Strickland, D.; Moffat, K.; Sosnick, T. R. *Proc. Natl. Acad. Sci. U. S.A.* **2008**, *105*, 10709–10714.
(81) Wu, Y. I.; Frey, D.; Lungu, O. I.; Jaehrig, A.; Schlichting, I.; Kuhlman, B.; Hahn, K. M. *Nature* **2009**, *461*, 104–108.
(82) Möglich, A.; Ayers, R. A.; Moffat, K. *J. Mol. Biol.* **2009**, *385*, 1433–1444.
(83) Arents, J. C.; Perez, M. A.; Hendriks, J.; Hellingwerf, K. J. *FEBS Lett.* **2011**, *585*, 167–172.
(84) Purcell, E. B.; McDonald, C. A.; Palfey, B. A.; Crosson, S. *Biochemistry* **2010**, *49*, 6761–6770.